Journal of Statistical Physics, Vol. 107, Nos. 1/2, April 2002 (© 2002)

Lateral Migration and Orientation of Elliptical Particles in Poiseuille Flows

Dewei Qi,[1] Lishi Luo,[2] Raja Aravamuthan,[3] and William Strieder[4]

Received February 16, 2001; accepted October 5, 2001

The simulations of elliptical particles in a pressure driven flow are performed using a lattice Boltzmann (LB) method. Effects of multi-particle interaction on the lateral migration and orientation of both neutrally and non-neutrally buoyant particles are investigated. Low and itermediate solid concentrations in terms of area fraction $f_a = 13$, 25, and 40% are included in these simulations.

KEY WORDS: Lattice Boltzmann simulation; elliptical particles; particle suspension; lateral migration; particle orientation; molecular dynamic simulation.

1. INTRODUCTION

Particle suspensions in pressure driven flows are found in many industrial applications such as, transport and refining petroleum, the paper manufacturing, pharmaceutical processing and environmental waste treatment. Since an understanding of the lateral migration, orientation and spatial distribution of particles in the pressure driven flows will help in designing and developing reasonable and economic industrial process, research has been focused on the investigation of the dynamic behavior of suspensions in the Poiseuille flow for many years.

Segre and Silberberg (1961, 1962) found that a neutrally buoyant particle will migrate to an equilibrium position between the wall and the channel

[1] Department of Paper and Printing Science and Engineering, Western Michigan University, Kalamazoo, Michigan 49008; e-mail: qi@lab2.cc.wmich.edu

[2] ICASE, NASA Langley Research Center, Hampton, Virginia 23681.

[3] Department of Paper and Printing Science and Engineering, Western Michigan University, Kalamazoo, Michigan 49008.

[4] Department of Chemical Engineering, University of Notre Dame, Notre Dame, Indiana 46556.

0022-4715/02/0400-0101/0 © 2002 Plenum Publishing Corporation

center due to wall effects, velocity profile curvature and shear force. This phenomenon, attributed to the nonlinear influence of inertia, has been confirmed by theoretical and experimental studies [Brenner (1966); Cox and Mason (1971); Leal (1980); Feuillebois (1989)] and more recently direct simulations [Feng, Hu, and Joseph (1994a, b); Huang, Feng, and Joseph (1994)].

Feng, Hu, and Joseph (1994a, b) have simulated the motion of a single circular particle in planar Poiseuille flow using a finite element method. Both neutrally and non-neutrally buoyant cases were examined. For a neutrally buoyant particle, the Segre–Silberberg phenomenon was re-produced in their simulations and they found that the equilibrium position is closer to the wall for a higher flow velocity. For a non-neutrally buoyant particle, when the density difference between the solid particle and the fluid is small, the equilibrium position is either close to the wall or to the centerline, depending on whether the particle leads or lags the local fluid. When the density difference is large enough, the particle, either lighter or heavier than the fluid, will move to the centerline. In general, a difference in the relative velocity across a solid particle may drive the particle to move laterally since the side with a higher relative velocity may lead to a lower pressure. Therefore, Joseph's group suggested that four mechanisms are responsible for the motion in the Poiseuille flows: wall lubrication repulsion; inertial lift due to shear slip; a lift due to particle rotation; a lift associated with the curvature of the undisturbed velocity profile.

Little information on the motion of elliptical particle in a pressure driven flows is available in literature. In the present paper, we will report the results of simulations for elliptical multi-particles in the pressure driven Poiseuille flow using a lattice Boltzmann (LB) method. Both neutrally and non-neutrally buoyant cases are investigated. Only low and intermediate solid concentrations in terms of area fraction $f_a = 13$, 25, and 40% are included in this report. Effects of multi-particle interaction on the migration and orientation of particles are also analyzed.

2. THEORY AND SIMULATION METHOD

The fluid flow is governed by the Navier–Stokes equations:

$$\rho_f \left(\frac{\partial \mathbf{u}}{\partial t} + \mathbf{u} \nabla \mathbf{u} \right) = -\nabla P + \eta \nabla^2 \mathbf{u} + \rho_f \mathbf{g} \tag{2.1}$$

where $\mathbf{u}$ is the velocity of fluid; P is pressure; η is the viscosity of fluid; ρ_f is the density of fluid; $\mathbf{g}$ is the acceleration of gravity.

The equations of the motion of solid particle are

$$M\frac{d\mathbf{U}}{dt} = M\mathbf{g} + \mathbf{F} \tag{2.2}$$

and

$$\mathbf{I}\frac{d\mathbf{\Omega}}{dt} = \mathbf{T} \tag{2.3}$$

where M is the mass of the solid particle; $\mathbf{U}$ is the velocity of the solid particle, $\mathbf{I}$ is the inertia; $\mathbf{F}$ and $\mathbf{T}$ are the hydrodynamic force and torque, respectively, on the solid particle.

The Navier–Stokes equations can be simulated by a lattice Boltzmann method [Wolframe (1986); d'Humieres, Lallemand, and Frisch (1986); McNamara and Zanetti (1988); Luo (1998); He and Luo (1997); Ladd (1994a, b); Koch and Ladd (1997); Aidun and Lu (1995); Aidun, Lu, and Ding (1998)]. The motion of nonspherical solid particles can be handled by molecular dynamic simulation [Qi (1997a, b, 1999)]. In particular, the LB method has been used to simulate two-dimensional (2D) rectangular particles and three-dimensional (3D) beds of Cylinders in sedimenting flows [Qi (2000a, b)]. In these simulations, the numerical results agree with experimental results and the LB method has correctly captured the essential physics of particle interactions with fluid flows. Therefore, the same method will be utilized in this work. The detailed method has been reported elsewhere by Ladd (1994a, b), Aidun, Lu, and Ding (1988) and Qi (1999) and will not be repeated here. In the present work, it is assumed that when two particles collide, an elastic collision occurs. In other words, the elliptical particle translation and angular momentum is conserved in the collision. This hard shell scheme, developed by Rebertus and Sando (1977) in the field of molecular dynamic simulation and adopted by Qi (2001) for sedimenting cylinders, will be used in this work.

3. SIMULATIONS AND RESULTS

One can find that the Poiseuille flow is determined by four dimensionless groups [Joseph (2001)]

$$\rho_s = \frac{\rho_p}{\rho_f}, \qquad C = \frac{2a}{W}, \qquad R = \frac{\rho_f \gamma 4a^2}{\eta}, \qquad G = \frac{2a(\rho_p - \rho_f)\, g}{\gamma\eta} \tag{3.1}$$

where ρ_s is the ratio of solid density ρ_p to fluid density ρ_f; W is the width of the channel; a is the radius of the principal axis of the elliptical particle; C is the confinement ratio, γ is the local shear rate of flow. R is the solid particle Reynolds number. In the Poiseuille flow, the shear rate $\gamma = \frac{4U_m}{W} - \frac{8U_m x}{W^2}$, which is not a constant and varies with coordinates x in the cross flow direction, where $\mathbf{U}_m$ is the maximum velocity of the undisturbed flow in the channel. We take the shear rate at $x = W/4$ to estimate the particle Reynolds number for all the cases in this work. The parameter

$$S = \frac{R}{G} = \frac{2a\gamma^2}{\left(\frac{\rho_p}{\rho_f} - 1\right)g} \tag{3.2}$$

measures the ratio of life to buoyant weight. The above non-dimensional parameters will be used in the later sections.

3.1. Neutrally Buoyant Elliptical Single Particle

Before investigating a multi-particle system, the migration of a singe elliptical particle is studied as the first step.

A simulation box size of 251×251 lattice unit is used. In this scale, the long radius of the ellipse is $a = 15$ and the short radius is $b = 7.5$. The confinement ratio $C = 0.12$ for all the cases. The flow and gravity are along the y-direction (down) as shown in Fig. 1. The bulk Reynolds number of suspension is defined by $\mathrm{Rb} = V_a W/v$, where V_a is the average velocity of the suspension and v is the kinematic viscosity.

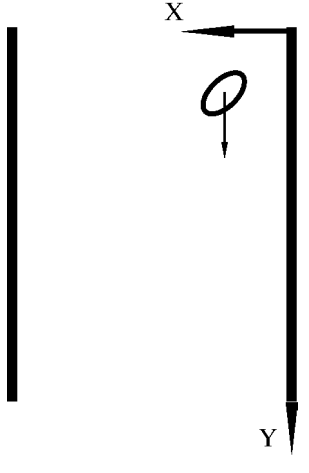

Fig. 1. Gravity and flows are in the y-direction (down).

Four simulations of a single neutrally buoyant elliptical particle, each with different initial positions in the x-direction or the cross flow direction, are performed at Rb = 140.625 first. Each of the four single elliptical particles migrates to the equilibrium position, which is $0.156W$ away from the wall. This final position is independent of the initial orientation and position as shown in Fig. 2. However, it takes much a longer time for a particle with an initial position closer to the center of channel to reach the same final position since the shear rate at the channel center is zero. The Segre–Silberberg phenomenon is found in the single elliptical particle system. The results show that the particle always lags the local flow and the effect of velocity curvature indeed pushes the particle toward the wall. This mechanism has been clearly explained by Feng, Hu, and Joseph (1994b).

The ellipse always rotates when it arrives at a final steady state or equilibrium state since the particle experiences a shear force. The angular velocity is a periodic function of time due to the shape. The rotation rate at the final equilibrium state is plotted in Fig. 3 for the neutrally buoyant particle.

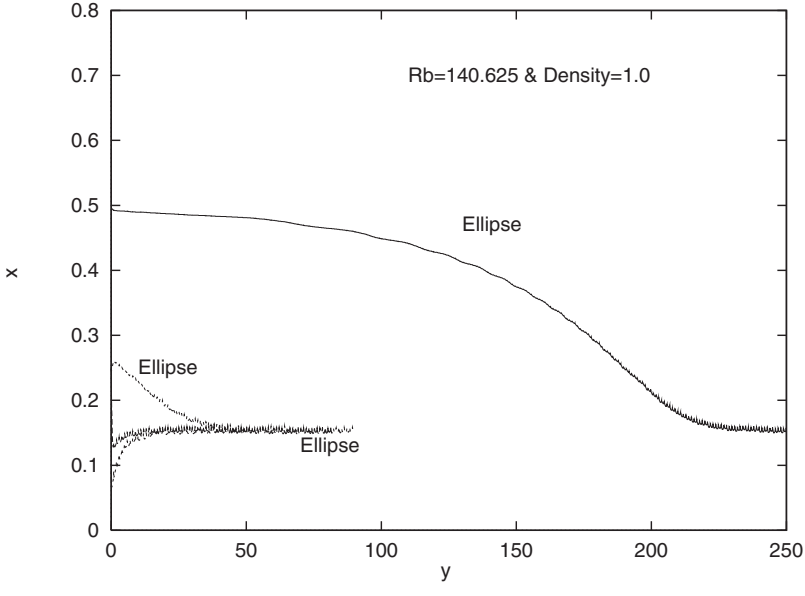

Fig. 2. The migration of neutrally buoyant single particle with different initial position is shown. There are four simulations for single ellipse at Rb = 140.625. All distances are normalized by the width of channel. The same is applied to other figures. The wiggles are caused by discrete solid particle.

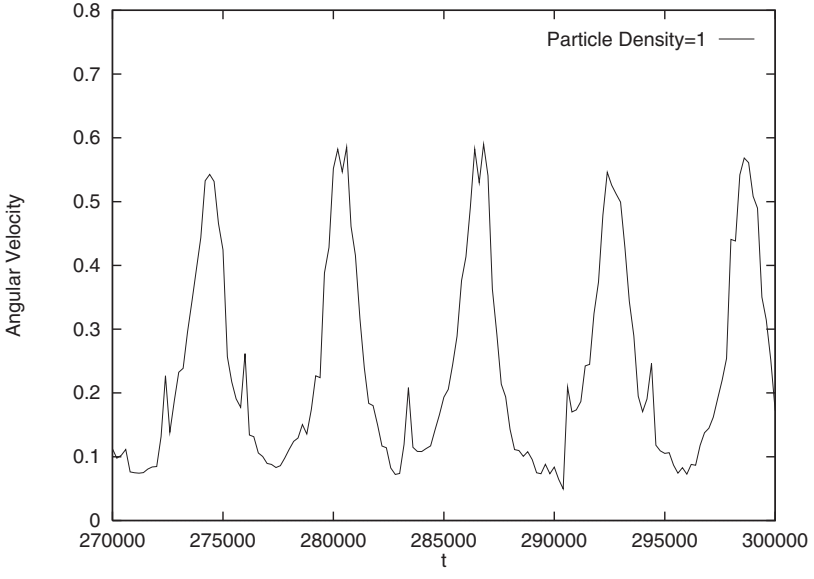

Fig. 3. The angular velocity as a function of time for a neutrally buoyant particle.

In order to describe the orientation of the ellipse, an angular distribution for a single particle is defined by $f(\theta) = \delta(\theta - \theta')$, which gives the probability of ellipse along angle θ per unit angle, where δ is a Dirac function and θ' is the angle of the particle at position $'$. The angular distribution function is normalized to one by integrating over an angle of π. It is shown in Fig. 4 that the probability of the orientation of elliptical particle on an average of time is much higher in the flow direction or y-direction than in the cross flow direction, since the ellipse experiences a smaller torque when the ellipse is instantly along the flow direction.

3.2. Non-Neutrally Buoyant Single Particle

When the solid density ($\rho_s = 1.005$, $R = 6.08$, and $G = 27.7$) is slightly larger than fluid density, the particle leads the local velocity of flow and the relative velocity at the right side of the particle is increased, resulting in a low pressure due to a higher relative velocity on this side. The particle migrates to the right wall due to the pressure difference and stabilizes at a position closer to the wall than does a neutrally buoyant particle. In this case the ratio of the lift to buoyant weight $S = 0.22$.

When the solid density ($\rho_s = 1.01$, $R = 6.08$, and $G = 55.4$) is sufficiently larger than the fluid density, the particle motion resembles sedimentation. The wall repulsion overwhelms the inertial lift and curvature

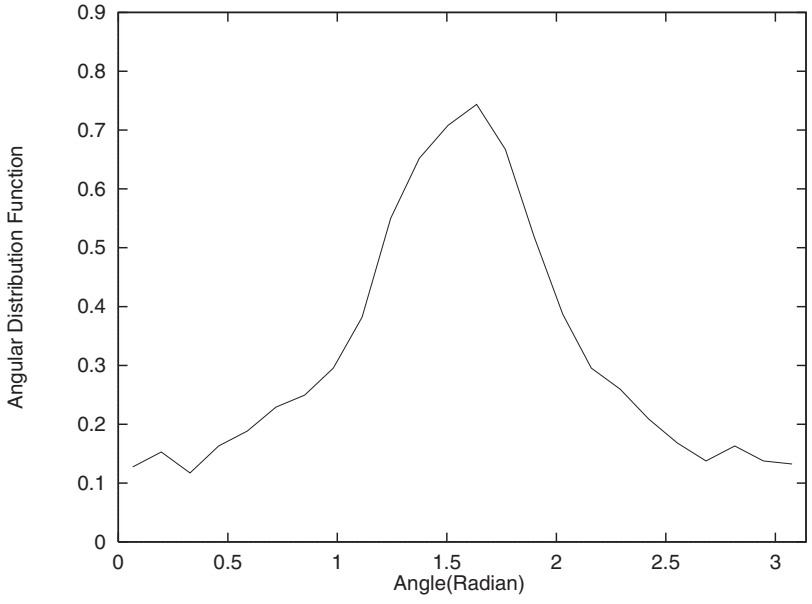

Fig. 4. The angular distribution function of neutrally buoyant particle.

effect, and the particle will move to the centerline. Figure 5 shows such two-directional migration for the cases of $\rho_s = 1.005$ and $\rho_s = 1.01$. For comparison purpose, the migration of the case of $\rho_s = 1.0$ is also shown in the same figure. It is not difficult to demonstrate that sedimentation is a major force to drive particles from the wall region to the central regions, when the density ($\rho_s = 1.01$) of ellipse is large enough. This can be seen more clearly from the angular distribution function. In a sedimenting flow, the orientation of an ellipse along the cross flow direction is dominated due to wake effects associated with nonlinear inertia. The angles of ellipse as a function of time are plotted in Fig. 6 for the cases of $\rho_s = 1.005$ and $\rho = 1.01$. Indeed, the ellipse of $\rho_s = 1.01$ turns to the horizontal direction or the cross flow direction quickly around $\theta = 0°$, while the ellipse of $\rho_s = 1.005$ turns approximately to the flow direction or vertical direction around $\theta = 83°$ with an oscillation. It is evident that the case of $\rho_s = 1.01$ is dominated by sedimenting effects since the particle has the feature of long body turning to horizontal direction and moving to the centerline. In fact, the shear rate is zero at the center of the channel. Contrary, the particle with $\rho_s = 1.005$ turns to the vertical direction and moves more closely to the wall. This behavior may be attributed to a mixture of the Poiseuille and sedimenting flows. The shear lift and wall effects cause the particle to be oriented in the

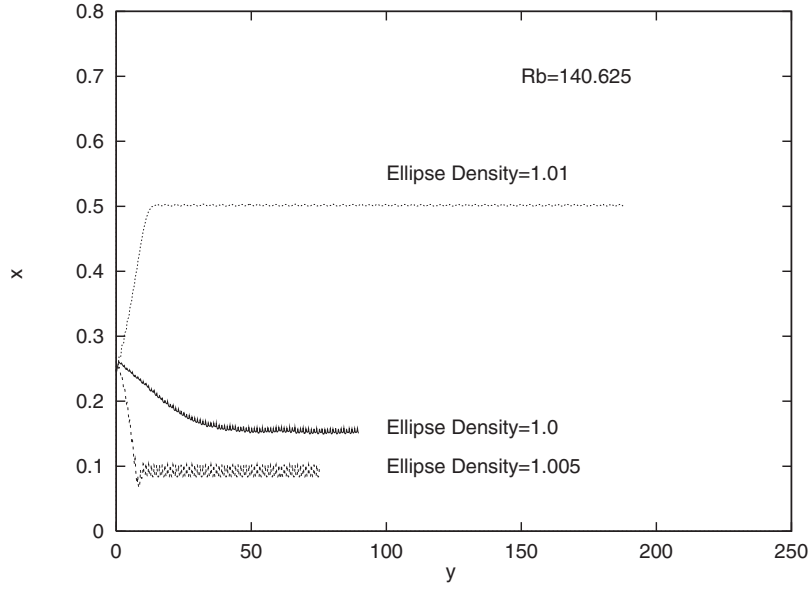

Fig. 5. The migration of ellipse with $\rho_s = 1.0$, 1.005, and 1.01 at $\mathrm{Rb} = 140.625$. The wiggles are caused by the discrete solid particle.

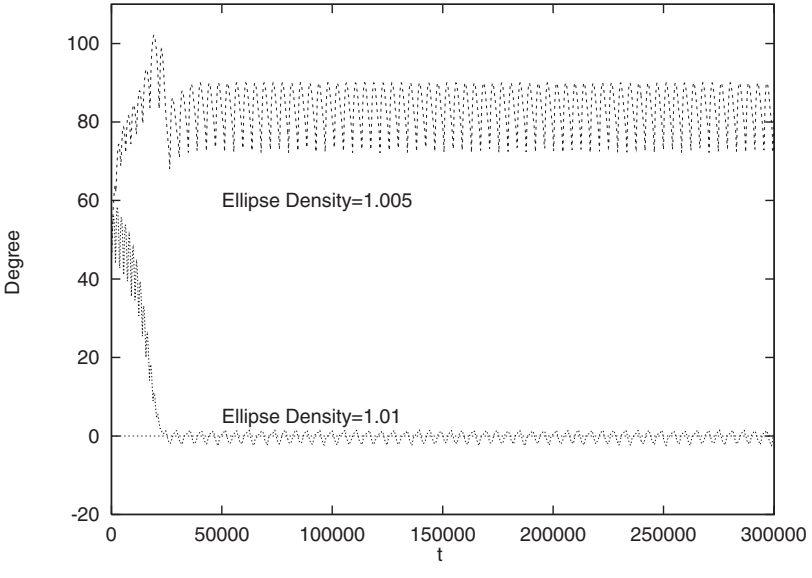

Fig. 6. The rotational angles of ellipse as a function of time for the cases of $\rho_s = 1.005$ and 1.01 at $\mathrm{Rb} = 140.625$.

vertical direction. Huang, Hu, and Joseph (1998) pointed out that the particle may turn to the vertical direction due to the wall effect at a small particle Reynolds number in a sedimenting flow. Similarly, the wall effect contributes to the orientation of the particle with $\rho_s = 1.005$. In these two cases, the particle rotation is stopped due to sedimenting and wall effects. However, the behavior of the rotation of a neutrally buoyant ellipse is entirely different from that of the two cases above. The particle is always rotated, while the probability of the orientation of the ellipse along the flow direction is much larger than that along the cross flow direction on an average of time, as pointed out before.

As previously mentioned, the neutrally buoyant particle slightly lags the local velocity in the undisturbed flow and the particle moves to the wall. When the particle ($\rho_s = 0.9995$, $R = 6.08$, $G = -2.77$) is lighter than fluid, the lagging velocity is increased. The relative velocity in the left of the particle (see Fig. 1) becomes larger, and the inertial lift pushes the particle to the direction of centerline. At even lighter particle density ($\rho_s = 0.995$, $R = 6.08$ and $G = -27.7$), the larger lagging velocity and strong wall repulsion force the particle to move across the centerline, where the particle experiences the same type forces in the opposite direction. Therefore, the particle swings back and oscillates around the centerline as shown in Fig. 7. Again, when sedimenting effect is dominant for the case of $\rho_s = 0.995$,

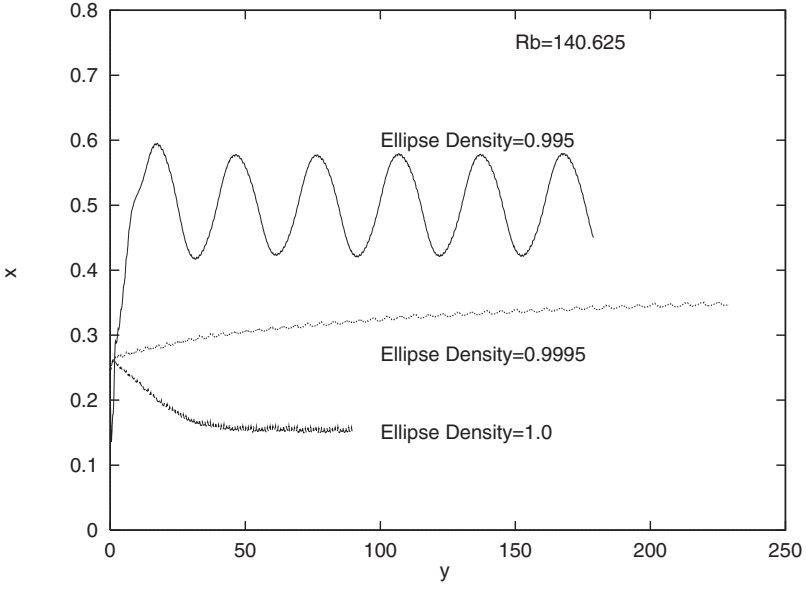

Fig. 7. The migration of ellipse with $\rho_s = 1.0$, 0.995, and 0.9995 at Rb = 140.625.

the particle rotation is stopped in a time average. While the particle is still rotating for the case of $\rho_s = 0.9995$ at the final state. In this case, the sedimenting does not overwhelm.

3.3. Neutrally Buoyant Multi-Particles

To study multi-particle interaction, motion of 23 neutrally buoyant elliptic particles in a pressure driven flow is simulated in the same box. In this case, the solid area fraction f_a is 13%; the bulk Reynolds number is 140.625. The configurations of particles at $t = 0$, $t = 300{,}000$ and $t = 400{,}000$ are shown in Fig. 8. It is clearly seen that the particles move to the

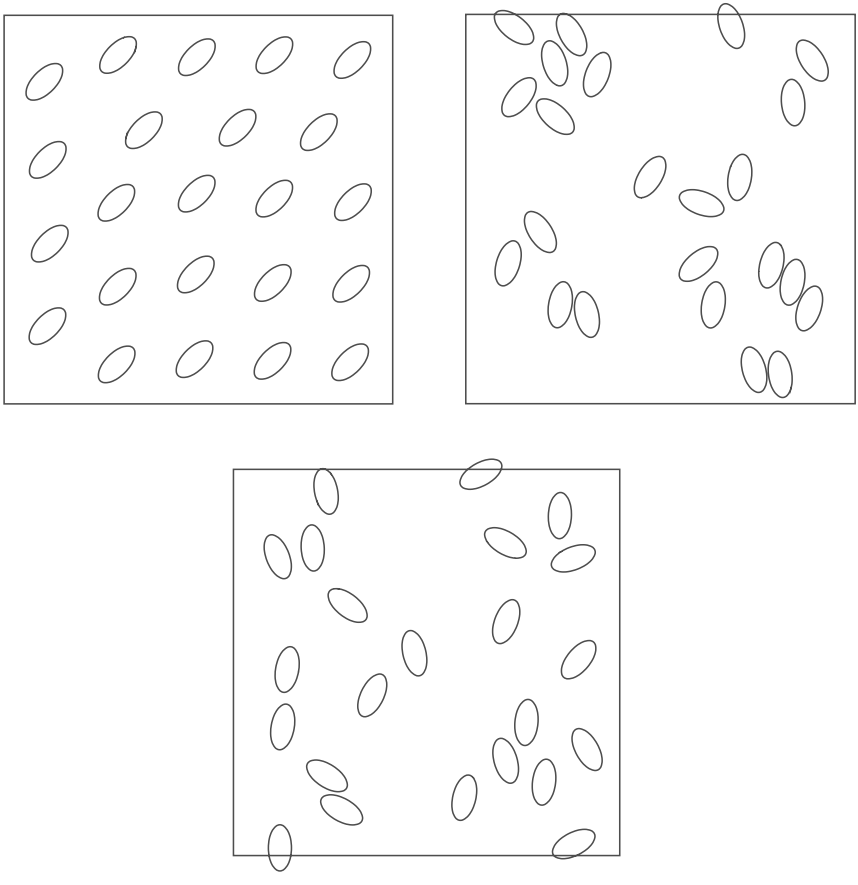

Fig. 8. The configurations and orientations of neutrally buoyant elliptical particles with the concentration of $f_a = 13\%$ at time steps $t = 0$ (the top left), $t = 300{,}000$ (the top right) and $t = 400{,}000$ (the bottom).

positions between the walls and the centerline. There are two maximum areas in the curve of solid fraction distribution on an ensemble average and these areas are located between the walls and centerline, as shown in Fig. 9. However, the maximum areas are closer to the centerline for the multi-particle system than for the single particle system since multi-particle interaction reduces the curvature effect. It seems that the particle clusters are formed and shown in Fig. 8. With a careful observation, it is found that there are two small shoulders at the velocity distribution function in Fig. 10. The locations of the shoulders on the velocity distribution curve correspond to the maximum areas on the solid fraction curve, indicating that the velocity of solid particles is suppressed at the high solid fraction area. This is expected because higher effective viscosity in this area reduces the velocity gradient.

Next, an angular distribution function is used to describe the orientation of multi-ellipses, which is defined by $f(\theta) = \frac{1}{N}\sum_i \delta(\theta - \theta_i)$, where N is the total number of particles and i indicates the ith particle. The results in Fig. 10 show that the elliptical particles have a much higher probability to be oriented in the flow direction than in the cross flow direction.

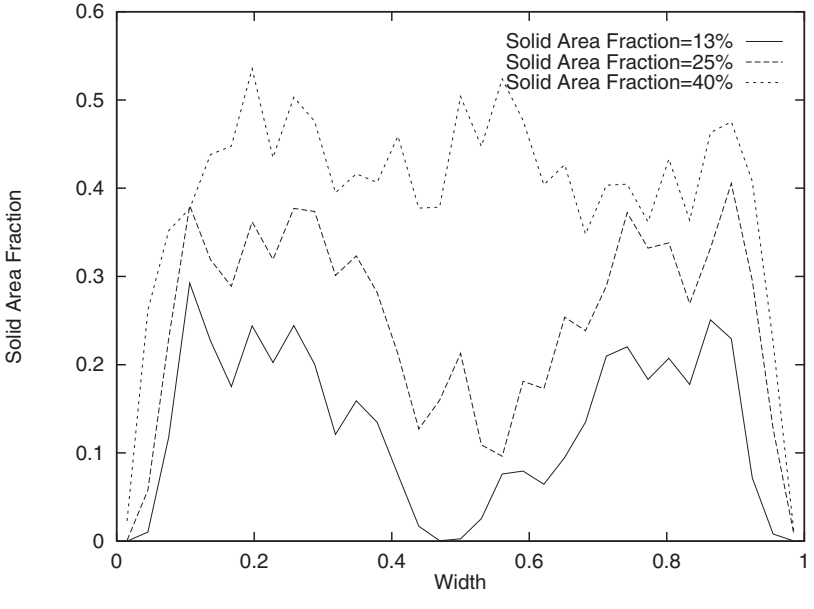

Fig. 9. The solid fraction distributions for $f_a = 13$, 25, and 40% at $\rho_s = 1.0$.

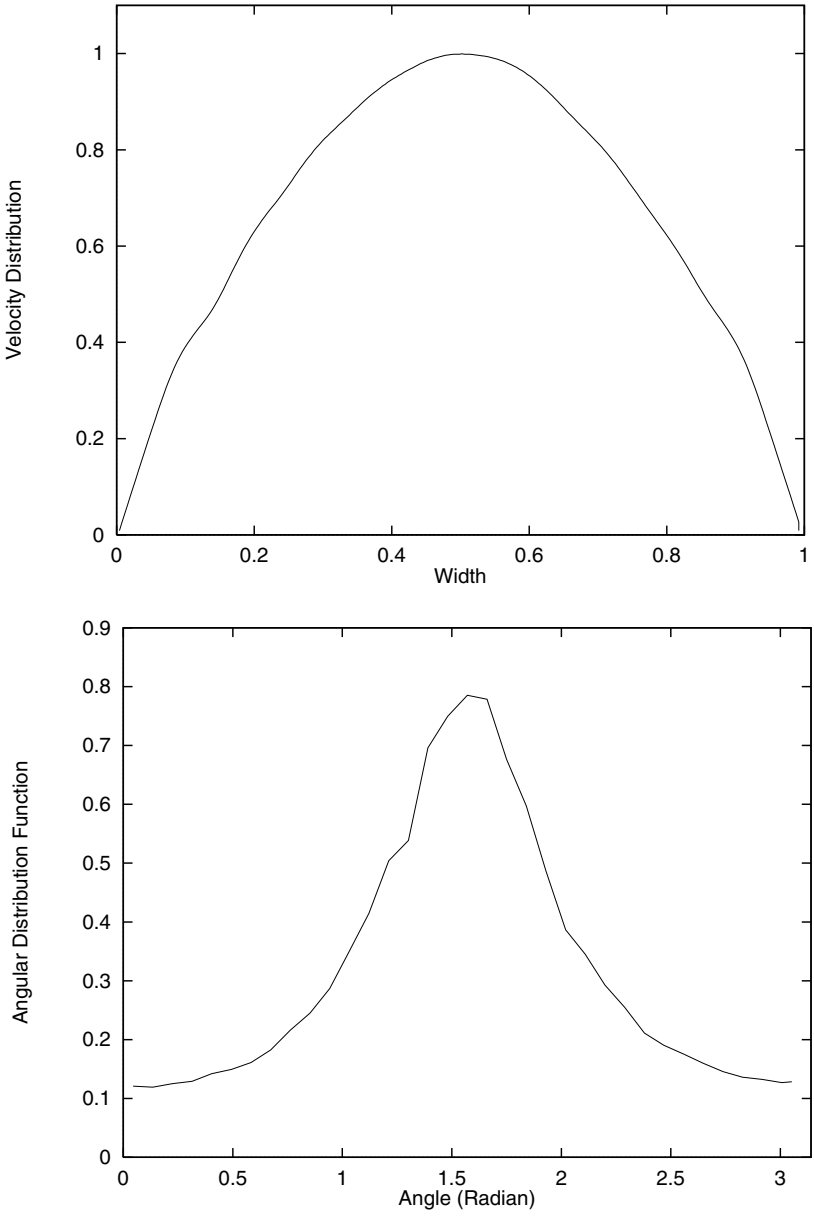

Fig. 10. The velocity distribution (top) and angular distribution function (bottom) for $f_a = 13\%$ and $\rho_s = 1.0$

To investigate the effect of the concentration of solid particles on migration, the simulations of 44 and 70 elliptical particles are conducted, in which the solid area fractions are 25 and 40%; and Rb is 71.81 and 75.78, respectively. The results show that the maximum areas on the curve of solid area fraction become broader and the minimum valley disappears when the concentration of solid particles increases (Fig. 9). It is observed that the rotation of a particle is also retarded by the existence of its neighboring particles. Thus, the lift due to rotation is reduced and solid particles may move more closely to the centerline. The velocity distribution of flow becomes blunt (Fig. 11). These results suggest that the Segre–Silberberg effect becomes weaker as the concentration of solids increases due to multi-particle interaction.

3.4. Non-Neutrally Buoyant Multi-Particles

When the density of solid particles ($\rho_s = 0.9995$) is smaller than that of flow, the two maximum areas between the walls and the centerline on the curve of solid area fraction become much wider (Fig. 12), as compared with the neutrally buoyant particles (Fig. 9). As the density of solid particles is continuously reduced to $\rho_s = 0.993$, the two maximum areas on the solid

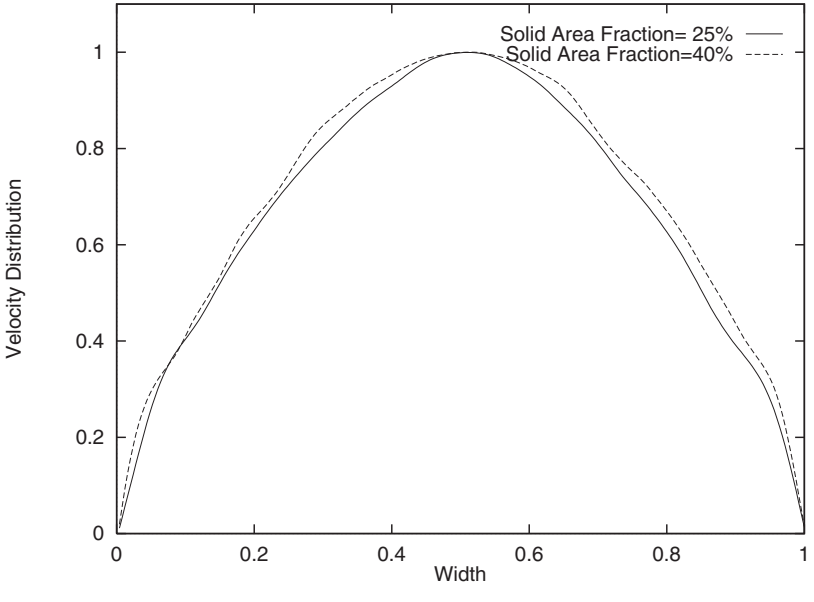

Fig. 11. The velocity distributions of neutrally buoyant multi-particles for the cases of $f_a = 25\%$ and $f_a = 40\%$. The velocity is normalized by the maximum velocity.

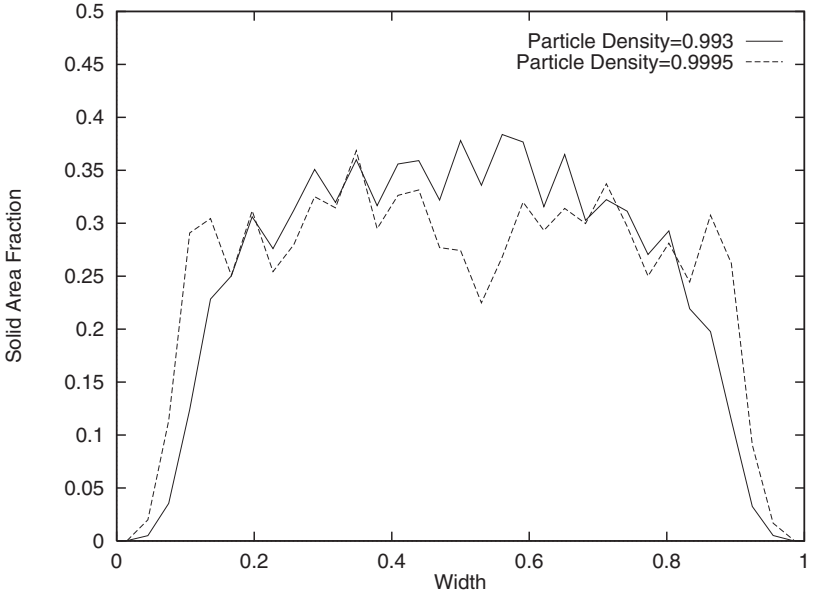

Fig. 12. The solid fraction distributions for elliptical particles with the densities of $\rho_s =$ 0.993 at $\mathrm{Rb} = 109.38$ and of $\rho_s = 0.9995$ at $\mathrm{Rb} = 129.7$. The solid area fraction for the two systems is $f_a = 25\%$.

fraction distribution curve are connected and the curve has a wide maximum area around the centerline as shown in Fig. 12. The two shoulders on the curve of velocity profile become more clear and the velocity profile becomes blunt as shown in Fig. 14. The orientation of ellipses along the flow direction is also greatly reduced in Fig. 13.

Finally, the cases of 44 solid particles ($f_a = 25\%$) with $\rho_s = 1.002$ and $\rho_s = 1.015$ are studied and compared with the same case except $\rho_s = 1.0$. When particles ($\rho_s = 1.002$) are slightly heavier than fluid, they move to the region more closer to the walls than do the neutrally buoyant particles due to the inertial lift forces. In this case, the behavior of multi-particles is similar to that of single particle. As seen in Fig. 15, the maximum areas of the curve of solid area fraction are located more closely to both sides of the walls for slightly heavier particles than for neutrally buoyant particles. As the solid density continuously increases to $\rho_s = 1.015$, more particles are shifted from the wall regions to the central region. Comparing the angular distribution functions between the case of neutrally buoyant particles and the case of heavier particles ($\rho_s = 1.015$) in Fig. 15, it can be seen that the orientation in the flow direction in the case of $\rho_s = 1.015$ is greatly reduced by sedimentation, which turns ellipses from the flow direction to the cross flow direction.

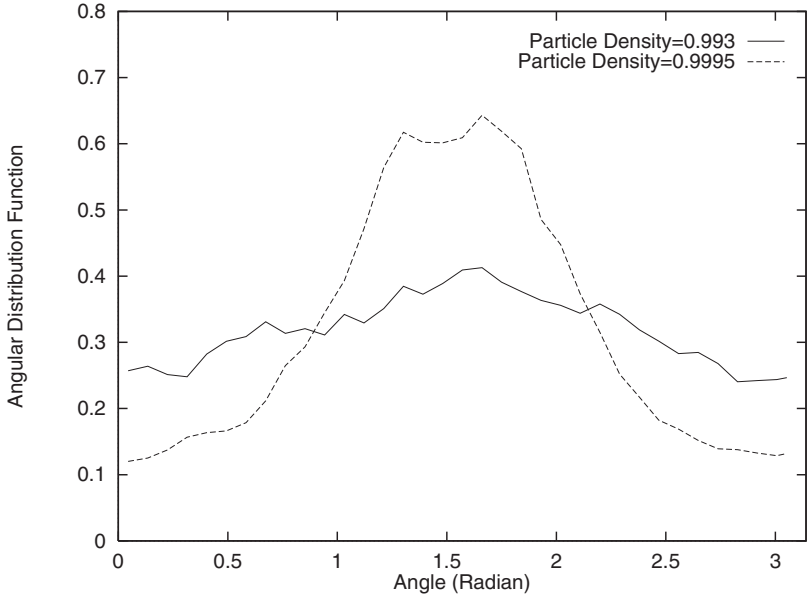

Fig. 13. The angular distribution functions for the same cases as in Fig. 12.

The inertial lift associated with curvature effect in this case still exist, but are relatively week. Therefore, the reasonable simulation results of solid area fraction, angular distribution function and velocity distribution in Figs. 15–17 can be attributed to a mixture of sedimenting and Poiseuille flows.

It is clear that the velocity profile in the case of $\rho_s = 1.015$ is broader than in the case of $\rho_s = 1.002$, and the velocity profile in the case of $\rho_s = 1.002$ is broader than in the case with neutrally buoyant particles.

4. CONCLUSIONS

The lattice Boltzmann method has been employed to simulate the dynamic migration and orientation behavior of single and multi elliptical particles in the planar Poiseuille flows. The difference between buoyant and non-buoyant particles on their lateral migration is analyzed. The solid concentrations, in terms of an area fraction, at 13, 25, and 40% are covered in the simulations. Several conclusions can be drawn from this work.

(a) For neutrally buoyant elliptical particle system, the Segre–Silberberg phenomenon is clearly observed in the simulations. A single elliptical particle migrates to an equilibrium position between the walls and the centerline of channel due to the inertial lift associated with the curvature of

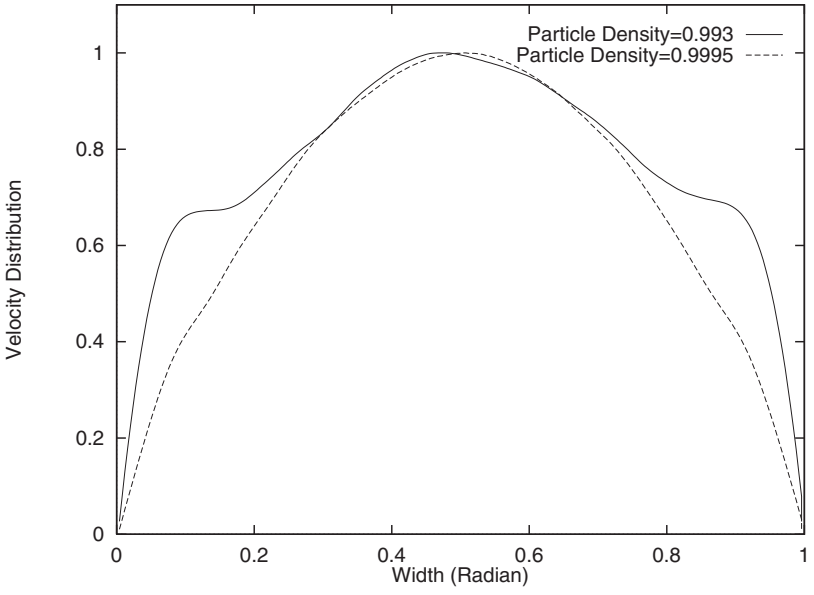

Fig. 14. The velocity distributions for the same cases as in Fig. 12.

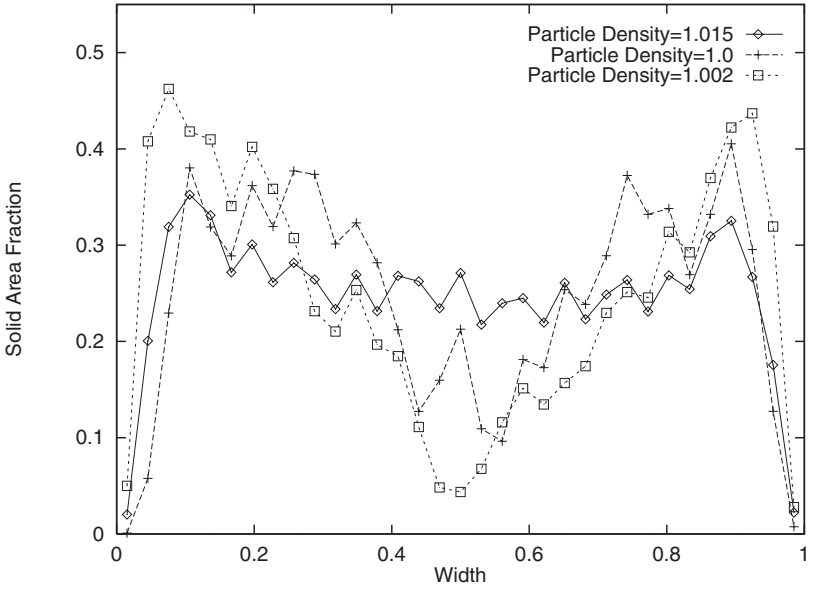

Fig. 15. The solid fraction distributions for elliptical particles with the density of $\rho_s = 1.0$ at $\mathrm{Rb} = 75.78$, of $\rho_s = 1.002$ at $\mathrm{Rb} = 82.81$ and of $\rho_s = 1.015$ at $\mathrm{Rb} = 114.06$. The solid area fractions for the three systems are the same at $f_a = 25\%$.

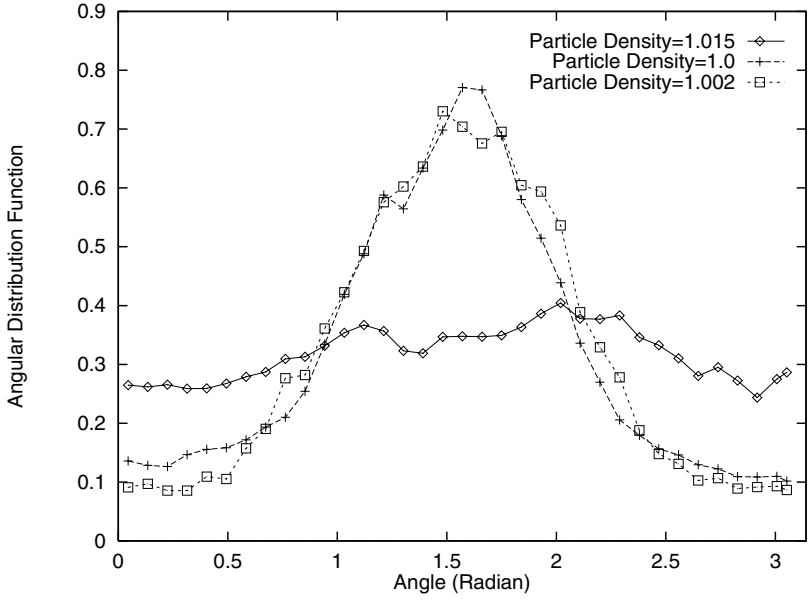

Fig. 16. The angular distribution function for the same cases as in Fig. 15.

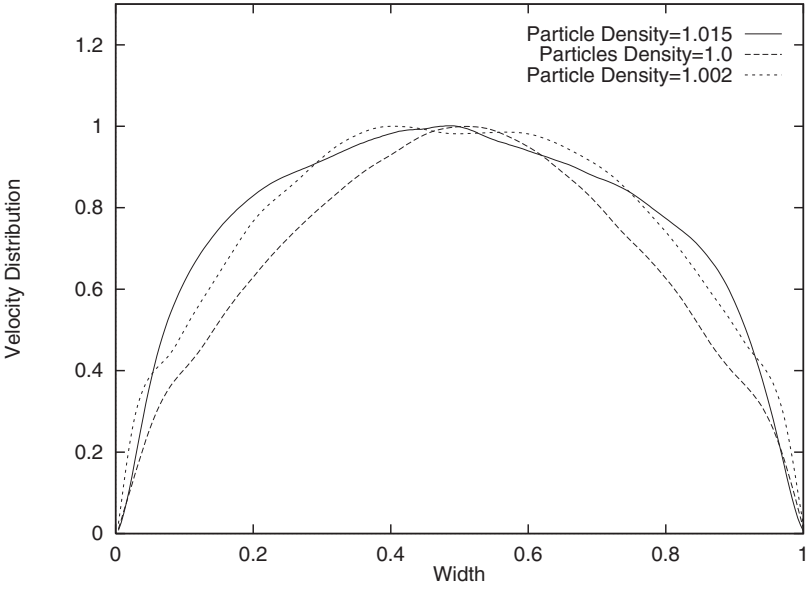

Fig. 17. The velocity distribution function for the same cases as in Fig. 15. The profile is normalized by the maximum velocity of suspensions for each case.

velocity profile. The final position in the cross flow direction is independent of initial particle position and orientation. At a steady state, an ellipse has a much higher probability to be oriented along the flow direction than along the cross flow direction due to the particle experiencing a smaller torque when the long body is instantly along the flow direction. It is demonstrated that the Segre–Silberberg effect also exists in a multi-particle system and drives particles to the region between the walls and the centerline. As a result, the curve of solid area fraction has two maximum areas located at both side of the centerline and has one minimum valley at the centerline. The curve of velocity profile has two shoulders corresponding to the maximum areas on the curve of solid area fraction. As the concentration of solid particles increases, the maximum areas on the curve of solid area fraction become wider and the minimum valley disappears. Meanwhile, the shoulders on the curve of velocity profile become more clear and the velocity profile becomes blunt. It is clear that the Segre–Silberberg phenomenon in a elliptical particle system is caused by wall lubrication repulsion, an inertial lift due to shear slip, a lift due to rotation and a lift associated with velocity curvature. However, the Segre–Silberberg effect is greatly reduced and virtually disappears as the solid area fraction increases to above 40% since multi-particle interaction changes velocity profile and reduces rotation. Ellipses are preferentially oriented along the flow direction at the simulated solid concentrations.

(b) When solid density is slightly larger than fluid, a single particle leads the flow and moves to a position closer to the walls since the inertial lift points to the wall. When the solid density is large enough, the particle moves back to the centerline. In this case, the slip velocity overshadows the effect of the velocity profile. The wall lubrication repulsive force becomes dominant and the particle motion is similar to sedimentation. The ellipse turns to the cross flow direction. The behavior of the two-way migration of the ellipse is the same as that found by Feng, Hu, and Joseph (1994a, b) and Huang *et al.* (1994, 1998) for a circular particle. This two way-migration behavior is maintained in a multi-particle system, i.e., particles move to the region closer to the walls, when particles are slightly lighter than the fluid, and move back to the centerline when particles are heavy enough. The orientation of ellipses along the flow direction is greatly reduced due to sedimentation effect.

(c) When the solid density is smaller than the fluid density, a particle lags the velocity of flow, the inertial lift and wall repulsion grow and push the particle to the centerline. As the density difference between solid particle and fluid increases, the particle is concentrated at the centerline region. Oscillations about the centerline are observed. For multi particle simulations, the

maximum on the curve of solid area fraction increases, while both the velocity profile and angular distribution function become blunt due to buoyant forces and multi-particle interactions.

ACKNOWLEDGMENTS

Acknowledgment is made to the donors of The Petroleum Research Fund, administered by the ACS, for support of this research. The computation time awarded by National Computational Science Alliance, NERSC, and Pittsburgh Supercomputing Center is appreciated.

REFERENCES

C. K. Aidun and Y. Lu, Lattice Boltzmann simulation of solid suspensions with impermeable boundaries, *J. Statist. Phys.* **81**:49 (1995).

C. K. Aidun, Y. Lu, and E. Ding, Direct analysis of particulate suspensions with inertia using the discrete Boltzmann equation, *J. Fluid Mech.* **373**:287 (1998).

H. Brenner, Hydrodynamic resistance of particles at small Reynolds numbers, *Adv. Chem. Eng.* **6**:287 (1966).

R. G. Cox and S. G. Mason, Suspended particles in fluid flow through tubes, *Ann. Res. Fluid Mech.* **3**:291 (1971).

D. d'Humieres, P. allemand, and U. Frisch, Lattice gas model for 3D hydrodynamics, *Europhys. Lett.* **2**:291 (1986).

J. Feng, H. H. Hu, and D. D. Joseph, Direct simulation of initial value problems for the motion of solid bodies in a Newtonian fluid. Part 1. Sedimentation, *J. Fluid Mech.* **261**:95 (1994a).

J. Feng, H. H. Hu, and D. D. Joseph, Direct simulation of initial value problems for the motion of solid bodies in a Newtonian fluid. Part 2. Couette and flows, *J. Fluid Mech.* **277**:271 (1994b).

F. Feuilleboisi, Some theoretical results for motion of solid spherical particles in a viscous fluid, in *Multiphase Science and Technology*, G. F. Hewitt *et al.*, eds., Vol. 4 (1989), pp. 583. Hemisphere.

P. Huang, J. Feng, and D. Joseph, The turning couples on an elliptic particle settling in a vertical channel, *J. Fluid Mech.* **271**:1–16 (1994).

P. Y. Huang, H. H. Hu, and D. D. Joseph, Direct simulation of the sedimentation of elliptic particles in Oldroyd-B fluids, *J. Fluid Mech.* **362**:297 (1998).

D. D. Joseph, http://www.aem.umn.edu/people/faculty/joseph (2001).

D. L. Koch and A. J. C. Ladd, Moderate Reynolds number flows through periodic and random arrays of aligned cylinders, *J. Fluid Mech.* **349**:31–66 (1997).

A. J. C. Ladd, Numerical simulations of particulate suspensions via a discretized Boltzmann equation. Part 1. Theoretical foundation, *J. Fluid Mech.* **271**:285 (1994a).

A. J. C. Ladd, Numerical simulations of particulate suspensions via a discretized Boltzmann equation. Part 2. Numerical results, *J. Fluid Mech.* **271**:311 (1994b).

L. S. Luo, Unified Theory of the lattice Boltzmann models for nonideal gases, *Phys. Rev. Lett.* **81**:1618–1621.

X. He and L. S. Luo, A priori derivation of the lattice Boltzmann equation, *Phys. Rev. E* **55**:R6333–R6336 (1997).

L. G. Leal, Particle motion in a viscous fluid, *Ann. Rev. Fluid Mech.* **12**:435 (1980).

G. McNamara and G. Zanetti, Use of Boltzmann equation to simulate lattice-gas automata, *Phys. Rev. Lett.* **61**:2332 (1988).

D. W. Qi, Non-spheric colloidal suspensions in three-dimensional space, *Internat. J. Modern Phys. C* **8**:4, 985–997 (1997a).

D. W. Qi, Computer simulation of coating suspensions. Proceedings, Tappi Advanced Coating Fundamental Symposium, May (Philadelphia, Pennsylvania, 1997b), pp. 201–211.

D. W. Qi, Lattice Boltzmann Simulations of particles in No-zero-Reynolds-number flows, *J. Fluid Mech.* **385**:41–62 (1999).

D. W. Qi, Lattice Boltzmann simulations of fluidization of rectangular particles, *Int. J. Multiphase Fluid* **26**(4):421–433 (2000).

D. W. Qi, Simulations of fluidization of cylindrical multi-particles in a three-dimensional space, *Int. J. Multiphase Fluid* **27**:107 (2001).

D. W. Rebertus and K. M. Sando, Molecular dynamic simulation of a fluid of hard spherocylinders, *J. Chem. Phys.* **67**:2585 (1977).

G. Segre and A. Silberbergi, Radial Poiseuille flows of suspensions, *Nature* **189**:209 (1961).

G. Segre and A. Silberbergi, Behavior of macroscopic rigid spheres in Poiseuille flow. Part 1, *J. Fluid Mech.* **14**:115 (1962).

S. Wolfram, Cellular automaton fluids 1: Basic theory, *J. Statist. Phys.* **45**:471 (1986).